Vol. 37 (2006) *ACTA PHYSICA POLONICA B* No 6

QMD APPROACH IN DESCRIPTION OF THE ^{18}O + ^{9}Be AND ^{18}O + ^{181}Ta REACTIONS AT $E_{\rm proj} = 35\,A$MeV

A.G. Artukh[a], A. Budzanowski[b], G. Kamiński[a,b] W. Kantor[b]
S.A. Klygin[a], E. Kozik[b†], O.V. Semchenkova[a], Yu.M. Sereda[a,c]
J. Szmider[b], Yu.G. Teterev[a], A.N. Vorontzov[a,c]

[a]Joint Institute for Nuclear Researches
141980 Dubna, Russia

[b]H. Niewodniczański Institute of Nuclear Physics PAN
Radzikowskiego 152, 31-342 Kraków, Poland

[c]Institute for Nuclear Research
Prospekt Nauki 47, 252650 Kiev-22, Ukraine

(Received October 29, 2005; Revised version received February 21, 2006)

Quantum Molecular Dynamics model was applied to reproduce the experimentally obtained charge, isotopic and velocity distributions of forward emitted fragments for the ^{18}O+^{9}Be and ^{18}O+^{181}Ta systems at $E_{\rm proj} = 35\,A$MeV. The charge numbers of the analyzed outgoing fragments were in the range of $Z = 2-11$ and $Z = 2-9$, respectively. The model taking into account the mutual two- and three-body effective nucleon–nucleon interactions and the short range of two body scattering appeared to be not completely suitable for the description of collisions leading to the forward emission of fragments.

PACS numbers: 25.70.–z, 24.10.Cn

1. Introduction

The energy of the projectile in heavy ion reactions studied in the past two decades subtends a wide range from a few MeV per nucleon up to energies exceeding $1\,A$GeV. In the low energy domain the relative velocities of colliding nuclei are small with respect to the internal Fermi motion of nucleons constituting heavy ions. This in turn causes that individual nucleon–nucleon interactions are hindered by the Pauli principle, so the nuclear interaction

† Corresponding author: `Ewa.Kozik@ifj.edu.pl`

at these energies is mostly understood in terms of the mean field approach. The peripheral and semiperipheral collisions lead to quasielastic and deep inelastic processes characterized by two massive, more or less excited fragments in the reaction exit channel, while the central and semicentral collisions lead to a fusion. The low energy reaction scenarios which clearly distinguish binary processes and the complete fusion become invalid at higher energies. At projectile velocity approaching the velocity of sound in nuclear matter (corresponding to energy around 14 AMeV) new processes do appear. These are noneqiulibrium emission of nucleons and clusters, projectile break-up and multifragmentation of the entire system, considered as a sort of liquid to gas phase transition of highly excited nuclear matter. At energies exceeding the Fermi limit ($E > 30\,A$MeV) the mean field role is significantly reduced and two-body interactions begin to take over. At energies above $\sim 100\,A$MeV the strength of the mean field becomes negligible in comparison to the single nucleon kinetic energy. In consequence the Pauli principle loses its blocking power, the mean free path for nucleon–nucleon collisions decreases and the intra nuclear cascade of collisions can develop. The variety of phenomena observed in heavy ion reactions depends not only on the energy but also on the impact parameter and mass available in processes.

In recent years a number of models has been developed to explain the mechanism of heavy ion reactions. These models may be divided into two basic categories. The first class of models is based on the assumption that the reaction mechanism is governed by mean field effects [1-3]. The individual nucleon–nucleon interactions are suppressed by the Pauli principle and the process is described by the one-body formalism. The second category of models assumes that heavy ion collisions proceed vastly by two-body interaction [4-8]. In between these extremes there are models linking the mean field and nucleon–nucleon dynamics [9-13].

Heavy ion reactions at intermediate energies, especially in the transitional Fermi energy domain, are of considerable interest both for studying of nuclear dynamics, such as compression and expansion modes, and for producing of secondary radioactive beams [14, 15]. The aim of these works is to answer the questions: *(i)* how rapidly does reaction mechanism evolve from low to high energy regime, *(ii)* does the neutron excess of the projectile and target influence the production of exotic nuclei, *(iii)* what a new phenomena can be met. In order to test our understanding of the heavy ion reaction mechanism in the Fermi energy domain, where the transition effects are expected to occur, the experimental data obtained for the ^{18}O (35 AMeV)+^{9}Be(^{181}Ta) reactions [16, 17] have been compared with model results employing the Quantum Molecular Dynamics [18] transport code.

The paper is organized as follows: Sec. 2 contains a brief description of the experimental set up and results, Sec. 3 contains a concise characteristics of applied model, in Sec. 4 the confrontation of the model results with experimental data and the discussion of findings are presented. Finally, conclusions are summarized in Sec. 5.

2. Experimental set up and results

The details of systematic investigations of forward-angle characteristics of isotopes with atomic numbers $2 \leq Z \leq 11$ produced in nucleus-nucleus collisions of the ^{18}O (35 AMeV) projectile on the ^{9}Be and ^{181}Ta targets are presented in Refs. [16, 17]. Measurements have been performed in the zero angle spectrometry mode using the in-flight fragment-separator COMBAS at the FLNR, JINR (Dubna) [19]. Two targets with different neutron-to-proton ratios were used to study the influence of the target neutron excess on the neutron-rich isotope production. The accuracy of the experimental data was limited by two factors: *(i)* the statistics and *(ii)* the accuracy of the determination of the charge of the ion beam passing through targets. The error connected with beam monitoring has been estimated to be not greater than 30%.

The forward-angle ($0^{\circ} - 2.5^{\circ}$) velocity, isotope and element distributions of species with $2 \leq Z \leq 11$ for the ^{18}O (35 AMeV)+^{9}Be reaction are presented in Figs. 2–6 of Ref. [16].

A simple correlation between the character of velocity spectra and the mass, charge number of fragment as well as the target size was found: *(i)* velocity distributions of products generated in the reaction on *tantalum* target are in general more narrow than in the case of *berylium* target. This indicates on less dissipative character of fragment production mechanism in the ^{18}O (35 AMeV)+^{181}Ta collisions, the low velocity component contributes to the total yield with less intensity. Irrespective of the used target: *(ii)* with decreasing value of isotope mass number at fixed Z-value the broadening of velocity distribution is observed, the bell shaped spectrum obtained for most neutron-rich isotope is replaced by more asymmetric shapes extending to lower velocities, *(iii)* the limits of velocity spectra depend on fragment charge number, the spread of distributions grows up with decrement of $Z_{\rm frag}$, *(iv)* the drift of maximum of velocity distribution towards lower velocity is observed for fragments resulting from bidirectional nucleon exchange (*e.g.* ^{18}C $(-2p, +2n)$,^{18}N $(-1p, +3n)$, ^{17}F $(-2n, +1p)$) and for fragments being net receptors (*e.g.* ^{19}O$(+1n)$,^{21}F$(+1p, +2n)$), *(v)* the positions of maxima of the fragment velocity distributions for the net donor species are concentrated at the value corresponding to the projectile velocity.

The experimental isotopic distributions were obtained by integration of the velocity spectra over the whole range of measured velocities. From the oxygen isotopic distribution the yield of ^{18}O products was excluded due to the impossibility of the separation of ^{18}O ejectile from ^{18}O projectile. For each Z element, excluding *helium*, the mass distributions are of the bell-like shapes. The most probable value of the detected mass, A, is close to the mass number of the isotope on the stability line.

For reactions induced on both targets (^{9}Be, ^{181}Ta) the element distributions are characterized by a sharp fall following the increment of product charge for $Z_{\rm frag} > Z_{\rm proj}$. With decreasing Z-value for $Z_{\rm frag} < Z_{\rm proj}$ the relatively stronger production of fragments for the ^{18}O+^{181}Ta reaction in the total yield is observed, although the general character of element distributions for both reactions is observed.

In the presence of unforeseen conformities of behavior of measured observables, irrespective of target size and target proton-to-neutron ratio, we have attempted to compare the experimental results with model prediction using the code, being the numerical realization of the Quantum Molecular Dynamics (QMD) model. The analysis of model results may be helpful in the interpretation of experimental data giving a reasonable explanation of encountered problems.

3. The CHIMERA code

CHIMERA (Code for Heavy Ion Medium Energy ReAction) is based on the QMD model of Aichelin [18] and the Quasi-Particle Dynamics model of Boal and Glosli [20]. The detailed description of the fundamental principles of the code is presented in [21], in this paper only a concise characteristic of the model is specified:

- the nucleons are represented by constant-width Gaussian wave packets, the time evolution of the centroids of the Gaussian wave packets is governed by two processes: the propagation due to the classical equation of motion (mutual two- and three-body effective nucleon–nucleon interactions) and the stochastic short range two body scattering (only the elastic channel of the nucleon–nucleon scattering is assumed);

- the scattering of nucleons is considered as if they were free, the collisions are statistically independent without the interference between different collisions;

- effective potential (nuclear effective potential derived from the Skyrme parameterization of the potential energy supplemented by the Coulomb potential and the momentum dependent Pauli potential to mimic the fermionic nature of the nucleons) replaces the real part of the transition matrix.

The dynamical evolution is stopped after a specified time and each nucleon is positioned in phase space. A cluster search routine allows to form clusters, when the nucleons are separated in the configuration space by less then 3 fm they are linked to form a cluster. Each cluster has assigned a mass number, atomic number, position, linear momentum, binding energy (excitation energy) and spin.

4. Model predictions

Calculations using the CHIMERA code were performed for the ^{18}O (35 AMeV)+^{9}Be and ^{18}O (35 AMeV)+^{181}Ta reactions assuming the hard EoS (nuclear matter compressibility $K = 330$ MeV). The number of considered events was 100000 and 150000, respectively. For the ^{18}O+^{9}Be reaction simulations using the soft EoS were also done. The comparison of the model charge distributions obtained for the hard and the soft EoS with the experimental data caused the choice the results of the hard EoS simulations for the further analysis. Using the assumption of the hard EoS the ratios of the production rates of fragments with $Z = 3$ and 9 to the yield of fragments with $Z = 7$ are closer to the experimental results than in the case of soft EoS. It was also stated that the simulations with the soft and the hard EoS produce quantitatively and qualitatively similar output results (velocity, charge, excitation energy distributions) not affecting the conclusions arising from the analysis. The dynamic evolution was stopped at 600 fm/c. The evolution of the reaction at the intermediate energy is dramatic in the short-time-scale phase (up to $\simeq$ 150 fm/c), after this time the variation of investigated quantities slows down and becomes smooth. However, a long-time scale evolution of the reaction may extend up to 3×10^{7} fm/c (10^{-16} s), so the choice of evolution time arises from the compromise between a weak dependence of investigated quantities on time in the second phase of reaction and an avoidance of extremely long computing time followed by increment of possible error propagation. Simulations were made in the full range of impact parameter, b, for ^{9}Be target $b = 0 \div 6$ fm ($R_{\mathrm{proj}} + R_{\mathrm{tar}}$=5.36 fm) and for ^{181}Ta target $b = 0 \div 10$ fm ($R_{\mathrm{proj}} + R_{\mathrm{tar}}$=9.44 fm). The studied results of simulations were limited to fragments appearing at the forward angles ($\theta_{\mathrm{lab}} \leq 5^{\circ}$ was chosen to obtain a sufficient statistics of analyzed model results) corresponding to the experimental conditions. The model predicted charge, mass and velocity distributions of fragments were compared to the experimental data.

4.1. ^{18}O *(35 AMeV)*+^{9}Be *reaction*

4.1.1. Element and isotope distributions

Fig. 1(a) presents the element distribution of forward emitted fragments predicted by the model (solid line). The dependence of the yields on fragment charge reaches the minimum for $Z = 3$, in the region of $Z = 4 \div 8$ the smooth increment of production rates is observed, for $Z > Z_{\rm proj}$ one can notice a sudden fall of yield. The products with $Z = 12$ corresponding to charge of the composite system, (CS), appear in the element distribution with a small probability. The calculated charge distributions corresponding to consecutive steps of impact parameter range are also shown in Fig. 1(a) (the legend is presented as inset in the figure). The correlation of the shape and magnitude of charge distributions with impact parameter is obvious. Fragments are produced mostly in collisions characterized by impact parameters $b = 1\div 4$ fm, the central collisions ($b = 0\div 1$ fm) give less contribution to the total charge distribution, although the shape of distribution is similar to that mentioned above. In the case of the most peripheral collisions the significant discrepancy of charge distribution shape is observed. Enhancement in the region of $Z = Z_{\rm proj}$ is anticipated, peripheral collisions correspond to the weak rearrangement of initial nucleon phase-space, in the final stage the most probably configuration corresponds to the input one. The absence

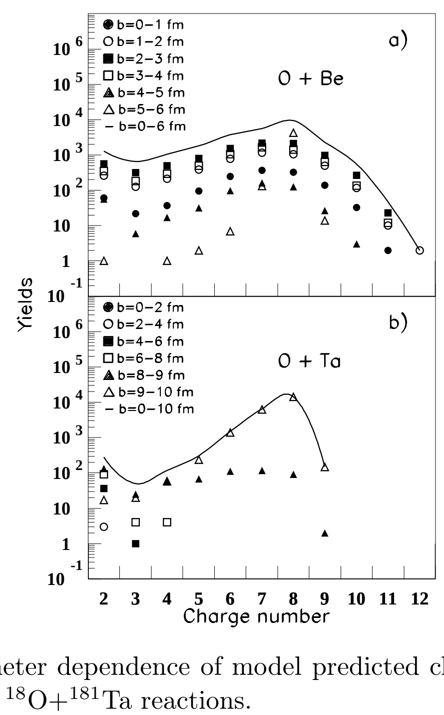

Fig. 1. Impact parameter dependence of model predicted charge distributions for (a) $^{18}O+^{9}Be$ and (b) $^{18}O+^{181}Ta$ reactions.

of distribution enlargement at $Z = Z_{\rm tar} = 4$ for products accompanying fragments with $Z_{\rm proj} = 8$ is connected with emission of *berylium* isotopes at angles $40° < \theta_{\rm lab} < 90°$. The multiplicity of fragments occurring in the exit channel, M, connected with gentle collisions reaches the maximum at the value equal to 2. More violent collisions taking place at lower values of impact parameter are the main source of fragments with $Z \neq Z_{\rm proj}$. These fragments originate mostly from collisions in which two or three massive fragments ($A_{\rm frag} \geq 2$) are accompanied by few free nucleons — neutrons and protons, the average multiplicity of events belonging to near-central collision class is equal to $M = 12$.

A comparison of the model predictions with the measured charge distribution for the ^{18}O (35 AMeV)+^{9}Be reaction shows that the model reproduces satisfactory the experimental results for ejectiles lighter than projectile in Z-space (Fig. 2(a)). The discrepancies appear for $Z \geq 10$, the model predictions overestimate the data. It results from the inherent feature of the model, the shortcoming of analysis is related to the scope of the model, which should be supplemented by the procedure deexciting hot primary fragments

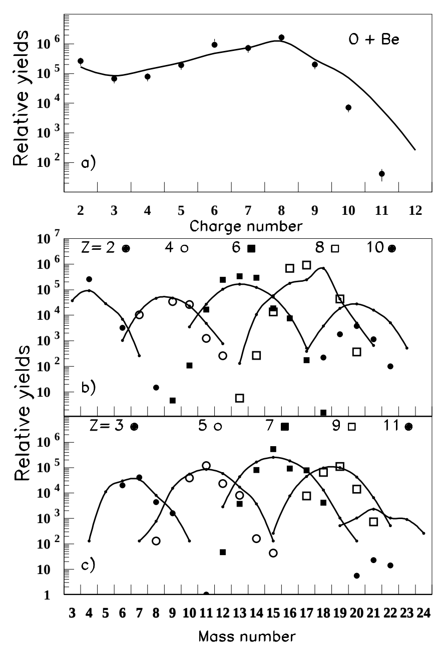

Fig. 2. Charge distribution (a) and the isotopic distributions (b), (c) for the ^{18}O+^{9}Be reaction. The solid curves correspond to the model results, the symbols represent the experimental data. Errors exceeding the size of data points are drawn in the Fig. 1(a).

offered by the code (CHIMERA determines the excitation energy and spin of fragments). Studies of the model correlation between excitation energy and charge of the ejectiles indicate on the continuous increment of fragment heating with the growing value of Z. The excitation energy of fragments with $Z = 2, 3$ does not exceed 20 MeV, while for elements with atomic number greater than Z_{proj} the heating may reach the value of 70 MeV. So, the element distribution may be corrected by the secondary evaporation having the greatest effect in the case of the most excited ejectiles with $Z > Z_{\mathrm{proj}}$. However, the heated prefragments, due to their low spin, decay predominantly by neutron emission not affecting the Z-value (a value on the average close to 15 MeV per one neutron emitted by hot nucleus is expected, taking into account the nucleon binding energy, the kinetic energy of evaporated nucleon and the energy carried away by γ-ray emission in the final stage of the fragment deexcitation). Concluding, in the region of lower atomic number, the element distribution is expected to be weakly affected by cooling the primary heavier fragments due to the spread the effects over the broad range of Z-values, the predominant neutron evaporation process and the relatively small probability of production of fragments heavier than projectile. Although fragments with $Z > Z_{\mathrm{proj}}$ are able to feed part of the element distribution for lower Z, resulting in the reduction of the number of heaviest ejectiles, causing the calculated distribution shape more adequate to the experimental one. The successful model description of the data may be an evidence of a weak importance of the secondary deexcitation process in the creation of charge distribution, but this assumption has to be justified by explicit inclusion of the secondary evaporation procedure in the calculations.

The model isotope distributions of elements with $Z = 2 \div 11$ emitted at forward angles for the $^{18}\mathrm{O}$ (35 AMeV)+ $^{9}\mathrm{Be}$ reaction are presented in Figs. 2(b), (c). The relative amplitudes and the positions of maxima of bell-shaped distributions predicted by the model reproduce satisfactory the experimental data for $Z = 2 \div 9$. The significant overestimation of relative isotope distribution yields for $Z = 10, 11$ isotopes, earlier manifested in the analyzed element distribution, is observed. For $Z \geq 5$ the widths of calculated distributions are greater in relation to the experimental correlations. A trend of stronger population of neutron-rich isotopes observed in the experimental data is preserved.

The correlation between the character of collision (more or less distant) and the neutron excess of fragments manifested by the N/Z-value was also studied. Model predicts that the isotopes with $A_{\mathrm{frag}} \leq 2\,Z_{\mathrm{frag}}$ are not propagated in distant collisions. On the contrary, neutron-rich fragments ($A_{\mathrm{frag}} > 2\,Z_{\mathrm{frag}}$) are produced in peripheral ($b > 5.5$ fm) and in more central collisions, mostly at $b = 1 \div 4$ fm.

4.1.2. Velocities of reaction products

Although the calculated mass ranges of isotope distributions correspond roughly to that obtained in the experiment, due to the insufficient yield of model predicted products, the analysis of fragment relative velocity, $v_{\mathrm{rel}} = v_{\mathrm{frag}}/v_{\mathrm{proj}}$, is confined to the most abundant isotopes. In Fig. 3 the relative velocity distributions of isotopes with $Z = 2 \div 10$ are presented. A direct comparison of experimentally obtained and calculated relative velocity distributions for a number of representative Z- and A-values of isotopes is shown in Fig. 4. The general trends observed in the experimental data are

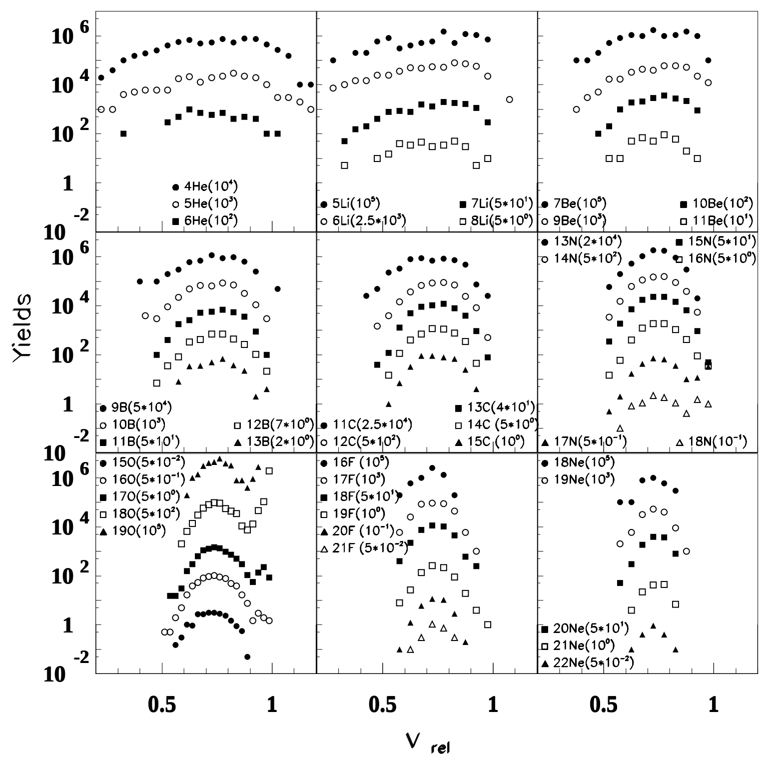

Fig. 3. Relative velocity distributions for fragments with $Z = 2 - 10$ resulting from CHIMERA code calculations for the ^{18}O+^{9}Be reaction. Panels present the distributions for He, Li, Be, B, C, N, O, F and Ne isotopes. The multiplication factors have been used to clarify the figures.

conserved in model predictions. The spread of calculated distributions grows up with the decrement of charge number of fragments. For the lightest isotopes ($Z = 2$) velocity distributions are spread over the range of $0.2 \div 1.2$, while for isotopes with $Z = 7, 10$ the limits of $0.5 \div 1.0$ and $0.55 \div 0.9$ are attained, respectively. The velocity distributions for the lightest isotopes

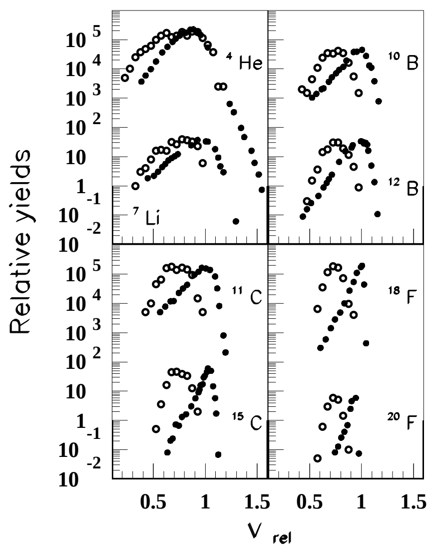

Fig. 4. Comparison of the experimental (full symbols) and calculated (hollow symbols) relative velocity distributions for ^{4}He, ^{7}Li, ^{10}B, ^{12}B, ^{11}C, ^{15}C, ^{18}F and ^{20}F produced in the ^{18}O+^{9}Be reaction. For clarity the confronted distributions are equalized in theirs maxima.

generated by the model ($Z = 2, 3$) are more flat, so the contribution of the low velocity part to the total yield is more significant than in the case of heavier products.

In opposite to the measured quantities the model velocity distributions are structureless, smooth and almost symmetric (except the cases of ^{16,17,18,19}O and ^{17,18}N). The upper velocity limit resulting from the model calculations is moved significantly towards lower value in relation to that obtained in the measurements (only velocities of *helium* isotopes predicted in the calculations exceed the projectile velocity) and, as a consequence, the maxima of model distributions are shifted down in comparison to the experimental ones. The maxima of the measured velocity distributions concentrate at the projectile velocity (except the fragments with $Z > Z_{\mathrm{proj}}$), the model, in average, predicts the maxima at value of $0.8\,v_{\mathrm{proj}}$. The special comment have to be dedicated to ^{16,17,18,19}O and ^{17,18}N isotopes. The bell-shaped velocity distributions predicted by the model are supplemented by the second component, the rapid enlargement of yield is observed in the vicinity of v_{rel} equal to 1. As it was discussed earlier these isotopes are generated in the most peripheral collisions corresponding to a little rearrangement of the initial phase space configuration and in less distant collisions being the main source of products with broad range atomic number ($Z = 2 \div 12$). In less distant collisions, despite of final result, the number of nucleons being submitted to numerically strong two-body interaction is meaningful, so the dissipation of energy (velocity) and conversion of the kinetic energy into the internal degrees of freedom is expected. At large impact parameter an unfrequent nucleon–nucleon interaction causes a weak phase-space rearrangement associated with conservation of initial physical features. So, the velocity, mass and charge of products are weakly changed in relation to projectile attributes (the enlargement of velocity distribution intensity at value corresponding to the projectile velocity).

It is difficult to expect that the inclusion of secondary evaporation will create the agreement of experimental and calculated results. Taking into account that light particles are evaporated isotropically in the rest frame of the emitters, the evaporation process does not affect the velocity vectors of the primary fragments averaged over a large number of events.

4.2. Comparison of model predictions for the ^{18}O (35 AMeV)+^{9}Be and ^{18}O (35 AMeV)+^{181}Ta reactions

For the ^{18}O (35 AMeV)+^{181}Ta reaction the model predicted charge distribution of primary fragments emitted at forward angles (Fig. 1(b)) is limited to $Z_{\rm frag} = 9$, the fragments with $10 \leq Z_{\rm frag} \leq 12$ occurring for reaction on ^{9}Be target are not generated. Only peripheral collisions ($b \geq 8$ fm) contribute to the total yield of the distribution of fragments with charge number $Z_{\rm proj} \geq 5$, the distant and less distant collisions ($b = 2\div$ 8 fm) are responsible for the production of the lightest fragments ($Z_{\rm frag} = 2, 3, 4$). For the ^{18}O+^{181}Ta collisions the reaction scenario corresponding to the production of forward emitted species occurs to be more simple than in the case of reaction on *berylium* target. Fragments originating mostly from peripheral collisions have projectile-like character (a removal of a few nucleons from the projectile). On the contrary for the ^{18}O (35 AMeV)+^{9}Be reaction more central collisions are responsible for fragment production. This dissimilarity causes the differences of relative velocity distributions (Fig. 5) observed also in the experimental data. The small rearrangement of nucleons connected with distant collisions is unable to influence significantly the velocity of fragment being the projectile remnant. Therefore, the velocity distributions are relatively narrow. The low velocity component is absent, the nucleon removal process is not able to diminish noticeably the final fragment velocity. For less distant collisions (substantial in the case of the ^{18}O+^{9}Be reaction) a considerable overlap of the projectile and the target nuclei causes that nucleons, due to the multiple mutual interactions, do not conserve their identities and the final fragment is composed from nucleons belonging in the initial stage to the projectile and to the target. The slow target nucleons (target is at rest, in the initial stage nucleons are equipped only with intrinsic momenta) are able to reduce considerably the final fragment ve-

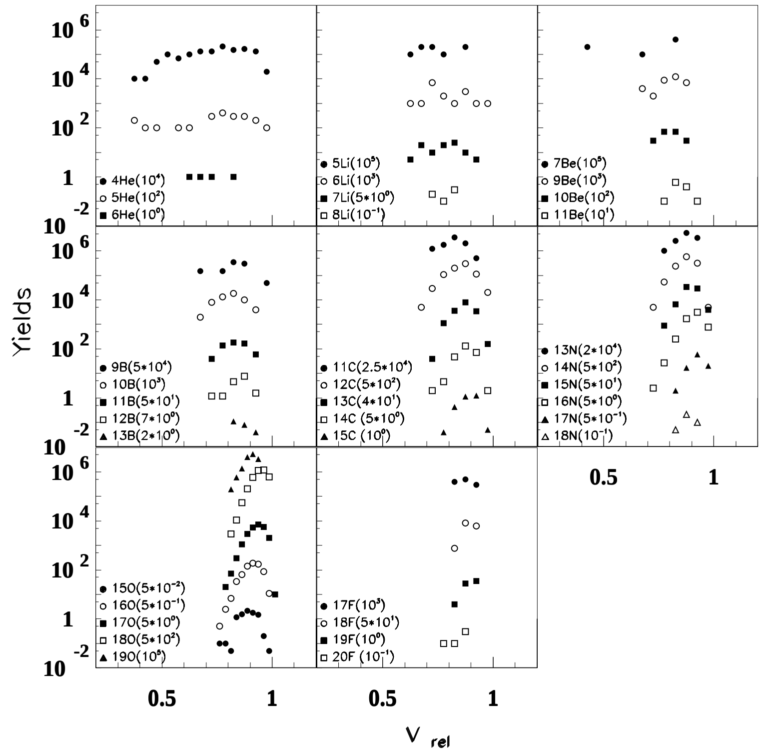

Fig. 5. Relative velocity distributions for fragments with $Z = 2$–9 resulting from CHIMERA code calculations for the ^{18}O+^{181}Ta reaction. Panels present the distributions for He, Li, Be, B, C, N, O and F isotopes. The multiplication factors have been used to clarify the figures.

locity, hence the relative velocity distributions of fragments, according to the experimental data, are broader for *beryllium* target than for *tantalum* target. On the other hand for both analyzed reactions the general trends of relative velocity distributions of isotopes are conserved, a broadening of distributions following the decrement of fragment charge and a shift of the upper limit of velocity distributions for $Z > Z_{\rm proj}$ toward the lower values is observed.

A comparison of the charge distribution shapes for both reactions (Fig. 1) indicates that for *tantalum* target the distribution is more pronounced near charge value equal to $Z = Z_{\rm proj}$ and the contribution for $Z_{\rm frag}$ far in the Z-space to the total distribution yield is relatively smaller for *tantalum* than for *beryllium* target.

It must be pointed out that the statistics for the ^{18}O (35 AMeV ^{181}Ta calculations ($\sim$ 150000 events) ought to be higher, especially taking into account the analysis of isotope relative velocity distributions. For isotopes with $Z < 6$ and $Z = 9$ the analysis and discussion are hindered because of an insufficient number of appropriate events. Unfortunately, the enormous calculation time for a system of nearly 200 nucleons is a drawback in generation of satisfactory statistics of the model predicted observables under consideration.

4.3. Discussion

For forward emitted fragments with charge number $2 \leq Z \leq 11(9)$ the QMD model calculations using CHIMERA code have been compared with the experimental results obtained for the ^{18}O (35 *A*MeV)+ ^{9}Be (^{181}Ta) reactions. Calculations have been performed in a broad range of impact parameter ($b = 0 \div R_{\text{proj}} + R_{\text{tar}}$, bdb weighted distribution), for each event with determined impact parameter the model has provided masses, charges, linear momenta, excitation energies and spins of final fragments.

The model predictions clearly show up quite good agreement with the experimental charge distribution for the ^{18}O (35 *A*MeV)+^{9}Be reaction and provides satisfactory the correlation between forward emitted fragment charge number *versus* the mass number. On the contrary the model description of experimentally obtained charge distribution for the ^{18}O (35 *A*MeV)+^{181}Ta reaction is not satisfactory, the measured distribution is significantly less pronounced in the vicinity of the charge number corresponding to Z_{proj} than the model predicted charge yield curve (Fig. 6). The normalization of calculated yield curve to the experimental distribution for the ^{18}O+^{181}Ta reaction was made on the ground of the scaling factor obtained for ^{18}O+^{9}Be (the experimental and calculated values of charge distribution were fitted at $Z = 7$). The normalization procedure of experimental and theoretical curves for ^{18}O+^{181}Ta results in rough conformity in the $Z = 4 \div 6$ interval inducing substantial overestimation of the experimental data for $Z = 7, 8$ and underestimation for $Z \leq 3$. In the face of successful for O + Be and unsuccessful for O + Ta model application one has to keep in mind that there is an essential difference between both reactions. The mass and charge number of final fragments is limited to the value of $A = 27$, $Z = 12$ and $A = 199$, $Z = 81$ (compound-nucleus-like remnant) in the case of the O + Be and O + Ta reactions, respectively. The model predicted charge distribution for reaction on *tantalum* target consists of two parts, the first located in the range of low Z values and the second spreads around the value equal to Z_{tar}. The heavy prefragments produced in complete/incomplete fusion processes with relatively high excitation energy and spin, by subsequent decay (emission of nucleons, light charged particles, light clusters, fission) are able to populate and depopulate different bins of charge yield curve. The excitation energy and the spin of the target remnant play an important role in the decay process. The differences between the average excitation energy removed by

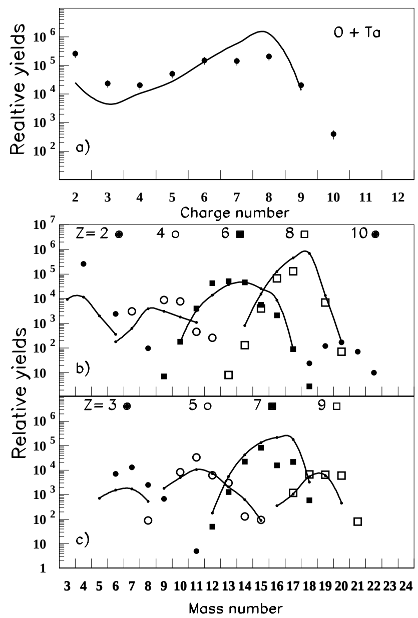

Fig. 6. Charge distribution (a) and isotopic distributions (b), (c) for the ^{18}O+^{181}Ta reaction. The solid curves correspond to the model results, the symbols represent the experimental data. Errors exceeding the size of data points are drawn in the Fig. 6(a).

emitted nucleons and particles (*e.g.* α particle) and the differences between the angular momentum carried away by these species define the character of the decay chain [22, 23]. Since the secondary processes influence the final charge (mass) spectra, the supply of QMD model calculations with procedure deexciting hot primary fragments is essential and meaningful to correct the $Z_{\rm frag}$ distribution for the $\mathrm{O} + \mathrm{Ta}$ reaction.

For validation of the above considerations the calculations using statistical model code GEMINI [24] were performed. The code employs a Monte Carlo technique to follow the decay chains of hot nuclei considering all possible binary divisions from light particle emission to symmetric division. As input for these calculations the initial population of nuclei, theirs excitation energies and spins resulted from the CHIMERA simulations were used. In Fig. 7 the calculated charge distributions of cold products for the ^{18}O+^{9}Be and ^{18}O+^{181}Ta reactions are compared to the experimental data and QMD model results. In accordance with expectations discussed previously, the inclusion of the sequential evaporation from the primary fragments in the analysis procedure causes the modification of the calculated element distributions. For the ^{18}O+^{9}Be reaction the agreement between the experimental data and the model results seems to be qualitatively worse, particularly in

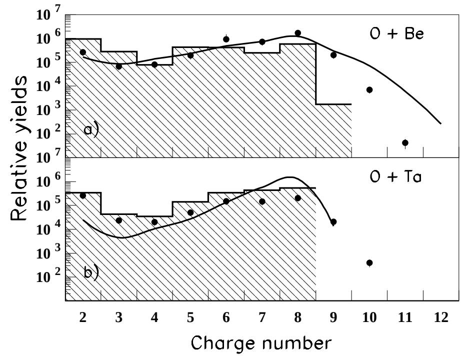

Fig. 7. Charge distribution for the (a)^{18}O+^{9}Be and (b)^{18}O+^{181}Ta reactions. Symbols correspond to the experimental data, lines and hatched histograms represent results of the CHIMERA and the CHIMERA + GEMINI calculations, respectively.

the range of $Z > Z_{\rm proj}$, although the dramatic change of the distribution shape for $Z \leq Z_{\rm proj}$ is not observed. Because of the substantial modification of element distribution for the ^{18}O+^{181}Ta reaction, the switching on of the secondary processes results in quite well description of the measured charge distribution in the range of $Z \leq Z_{\rm proj}$. Nevertheless, the accordance of the measured and the calculated element distributions using the tandem CHIMERA + GEMINI for the ^{18}O+^{181}Ta reaction does not testify to ability of the QMD approach in description of the experimental data.

The model predictions completely fail in the description of velocity distribution shapes, a two-component character of the experimentally obtained velocity distributions is replaced by more symmetric model distributions. For both reactions the inclusion of cooling procedure produces neglected effects in modifications of velocity distributions conserving the substantial discrepancy between data and model predictions. The enhanced role of the dissipative component of experimental velocity distributions following the decrement of isotope mass accompanied by a significant broadening of the distributions towards higher values of relative velocity, attaining for ^{4}He the value of $\simeq 1.5$ is not predicted by the model. Moreover, the maxima of the model predicted velocity distributions are shifted toward lower values in comparison to the experimental results. The velocities of fragments exceeding the projectile velocity observed in the experimental data for nearly all isotopes are generally not generated by the model (except the case of *helium* isotopes for *beryllium* target). The blatant disagreement of measured velocity distributions with the results of QMD calculations indicates that the mean field approximation using Skyrme (mutual two- and three-body) interaction, the momentum dependent Pauli potential and the Coulomb potential supplemented by collision term is not able to preserve the initial structure and properties of the colliding nuclei in forward emitted final fragments. The participating ions lose their identities what is manifested by the reduction of their velocities. In this type of the model calculations in the final stage of the reaction the number of nucleons of projectile-like fragments (PLF) belonged in the initial stage to the target is meaningful. It was found by Bordiere *et al.* [14] that the percentage of target nucleons in the final light fragments increases up to 50% even for intermediate values of impact parameters. Concluding it was found that for forward emitted fragments produced in reactions at energy close to the Fermi energy the QMD approach overestimates the contribution of dissipative processes. The experimental data indicate on more significant role of non-dissipative processes in fragment production manifested by positions of velocity distribution maxima. Processes of direct removal of a few nucleons from the projectile not diminishing the velocity of projectile remnant in relation to $v_{\rm proj}$ are beyond the limits of QMD approach.

The preliminary analysis of the model isotope production ratio for ^{9}Be and ^{181}Ta targets seems to confirm the experimental results, indicating on the correlation of $(N/Z)_{\rm frag}$ with $(N/Z)_{\rm tar}$ manifested by the enhancement of production ratio of neutron-rich isotopes on Ta and Be targets (Fig. 3 of Ref. [17]). This correlation is in accordance with the findings of Borrel *et al.* [25] that, irrespective of the target size, the isotopic distributions of fragments are sensitive to the target neutron to proton ratio, the neutron excess of the target is accompanied by a stronger abundance of neutron-rich fragments. The significant influence of the neutron skin of the target in the overlap zone with the projectile, where nucleon–nucleon collisions take place, causes this effect. Furthermore, for intermediate energy domain nucleon–nucleon cross section is three times larger for neutron–proton scattering than for neutron-neutron and proton–proton collisions [26]. The enhanced probability for collisions between protons of the projectile and neutron of the target intensifies the effect of proton-deficient fragment production on neutron-rich target.

5. Summary

In the paper we have presented a comparison of the experimental data for the ^{18}O (35 AMeV)+ ^{9}Be and ^{18}O (35 AMeV)+^{181}Ta reactions with theoretical results of QMD calculations. The results of calculations show that the QMD model is appropriate to describe only some experimental observables.

In the intermediate energy domain the clean picture of processes corresponding to the low energy regime (binary processes, mean field effects) or high energy region (fragmentation, two-body interactions) is impossible to apply. Disentangling the superposition of various processes is not an easy task in general, the identification of fragment production mechanism, especially from the inclusive measurements of single fragment, appears to be particularly difficult. However, we may take an advantage from the fact that the simulations performed using the predictive power model provide in principle much more information than the experiment. An additional information is *e.g.* the impact parameter dependence of the quantities under consideration. For the ^{18}O+^{9}Be and ^{18}O+^{181}Ta reactions the creation of fragments is controlled by the impact parameter. For ^{9}Be target the forward emitted prefragments are produced in violent and gentle collisions, on the contrary, for ^{181}Ta target the peripheral collisions are mostly responsible for the fragment formation.

The QMD model predictions for reactions on *berylium* target follow closely the experimental charge and isotope distributions. On the other hand no success was attained in reproduction of the experimental data for *tantalum* target. The deexcitation of primary nuclei expected to play a role in a fragment production yield improves the accordance of the measured charge distribution with the predictions for the ^{18}O+^{181}Ta reaction, getting worse the description for the ^{18}O+^{9}Be reaction. Similarities of the measured quantities (the isotope and velocity distributions of fragments) for both reactions confirmed by the model seem to be rather accidental because of completely different collision picture responsible for fragment formation. The general dependence of the model velocity distributions on the mass and charge of fragments is observed according to the experimentally obtained correlations (the broadening of the velocity distributions with decreasing of fragment charge number, the shift of maximum positions towards lower values for the fragments with $Z_{\rm frag} > Z_{\rm proj}$). Nevertheless, no success in the interpretation of the meaningful yields of fragments with velocities significantly exceeding the projectile velocity for $Z_{\rm frag} \leq Z_{\rm proj}$ has been attained. It is possible to draw the conclusion that for forward emitted fragments in the ^{18}O+^{9}Be and ^{18}O+^{181}Ta reactions the basic theoretical concepts used in the model is incorrect. Our results have shown that the QMD approach seems to overestimate the dissipative processes. A discrepancy between the experimental data and predictions of the model is a consequence of numerically strong nucleon–nucleon interactions and bidirectional flow of nucleons, even the net mass transfer is small, generating a meaningful energy dissipation in the final stage of collisions.

We are indebted to J. Łukasik who kindly provided us with the CHIMERA code. The authors are grateful to Yu.T. Oganessian for valuable discussions. This work was supported in part by grant RFPR-01-02-16427.

REFERENCES

[1] P. Bonche, S.E. Koonin, J.W. Negele, *Phys. Rev.* **C13**, 1226 (1976).

[2] S.E. Koonin, K.T.R. Davies, V. Maruhn-Rezwani, H. Feldmeier, S.J. Krieger, J.W. Negele, *Phys. Rev.* **C15**, 1359 (1977).

[3] K.T.R. Davies, S.E. Koonin, *Phys. Rev.* **C23**, 2042 (1981).

[4] Y. Yariv, Z. Fraenkel, *Phys. Rev.* **C20**, 227 (1979).

[5] J. Cugnon, *Phys. Rev.* **C22**, 1885 (1980).

[6] J. Cugnon, T. Mizutani, J. Vandermuelen, *Nucl. Phys.* **A352**, 505 (1981).

[7] J. Cugnon, *Nucl. Phys.* **A387**, 191c (1982).

[8] S.A. Bass, M. Belkacem *et al.*, *Prog. Part. Nucl. Phys.* **41**, 225 (1998).

[9] G.F. Bertsch, H. Kruse, S. Das Gupta, *Phys. Rev.* **C29**, 673 (1984).

[10] J. Aichelin, G.F. Bertsch, *Phys. Rev.* **C31**, 1730 (1985).

[11] H. Kruse, B.V. Jacak, J.J. Molitoris, G.D. Westfall, H. Stöcker, *Phys. Rev.* **C31**, 1770 (1985).

[12] C. Grégoire, B. Remaud, F. Sébille, L. Vinet, Y. Raffray, *Nucl. Phys.* **A465**, 317 (1987).

[13] C. Grégoire, D. Jacquet, M. Pi, B. Remaud, F. Sébille, E. Suraud, P. Schuck, L. Vinet, Y. Raffray, *Nucl. Phys.* **A471**, 399c (1987).

[14] B. Bordiere, M.F. Rivet, L. Tassan-Got, Internal Report IPNO-DRE-90-06.

[15] H. Fuchs, K. Möring, *Rep. Prog. Phys.* **57**, 231 (1994).

[16] A.G. Artukh, G.F. Gridnev, M. Gruszecki, F. Kościelniak, A.G. Semchenkov, O.V. Semchenkova, Yu.M. Sereda, J. Szmider, Yu.G. Teterev, *Phys. Atom. Nucl.* **65**, 393 (2002).

[17] A.G. Artukh, G.F. Gridnev, M. Gruszecki, F. Kościelniak, A.G. Semchenkov, O.V. Semchenkova, Yu.M. Sereda, J. Szmider, Yu.G. Teterev, *Nucl. Phys.* **A701**, 96c (2002).

[18] J. Aichelin, *Phys. Rep.* **202**, 233 (1991).

[19] A.G. Artukh, G.F. Gridnev *et al.*, *Nucl. Instrum. Methods* **A426**, 605 (1999).

[20] D.H. Boal, J.N. Glosli, *Phys. Rev.* **C38**, 1870 (1988); *Phys. Rev.* **C38**, 2621 (1988).

[21] J. Łukasik, Z. Majka, *Acta Phys. Pol. B* **24**, 1959 (1993).

[22] F. Rami, J.P. Coffin, G. Guillaume, B. Heusch, P. Wagner, A. Fahli, P. Fintz, *Nucl. Phys.* **A444**, 325 (1985).

[23] H. Ikezoe, N. Shikazono, Y. Tomita, K. Ideno, Y. Sugiyama, E. Takekoshi, *Nucl. Phys.* **A444**, 349 (1985).

[24] R.J. Charity, M.A. McMahan, G.J. Wozniak, R.J. McDonald, L.G. Moretto, D.G. Saratites, L.G. Sobotka, G. Guarino, A. Pantaleo, L. Fiore, A. Gobbi, K.D. Hildenbrand, *Nucl. Phys.* **A483**, 371 (1988).

[25] V. Borrel, B. Gatty, D. Guerreeau, J. Galin, D. Jacquet, *Z. Phys.* **A324**, 205 (1986).

[26] B.G. Harvey, *Nucl. Phys.* **A444**, 498 (1985).